IEEE Access
Multidisciplinary | Rapid Review | Open Access Journal

Received December 20, 2021, accepted December 28, 2021, date of publication January 7, 2022, date of current version March 11, 2022.

Digital Object Identifier 10.1109/ACCESS.2022.3141312

Novel Method for Estimating Utility Harmonic Impedance for a Direct-Drive Permanent Magnet Synchronous Generator Wind Farm

RUNZE ZHOU, XIAOYANG MA, RUI XU, XIANYONG XIAO, AND JINSHUAI ZHAO
College of Electrical Engineering, Sichuan University, Chengdu 610065, China

Corresponding author: Xiaoyang Ma (mxy_scu@163.com)

This work was supported in part by the Interdisciplinary Innovation Cultivate Project of Sichuan University under Grant 0030304153003, and in part by the Open Fund of State Key Laboratory of Power System and Generation Equipment Tsinghua University under Grant SKLD21KM04.

ABSTRACT Accurate estimation of the utility harmonic impedance is significant for harmonic control and responsibility division. Traditional methods of estimating the utility harmonic impedance are valid on the premise that the harmonic impedance on the wind-farm side is significantly greater than that on the utility side. However, with the installation of filters and reactive power compensation devices in wind farms, traditional estimation methods are no longer applicable. The accuracy of most existing estimation methods depends only on the accuracy of the model. This can cause large errors in the estimation of the utility harmonic impedance on a wind farm. To address this challenge, this paper proposes a method for estimating the utility harmonic impedance for a direct-drive permanent magnet synchronous generator wind farm based on a modified model with measured data. The proposed method uses the measured data to modify a model to obtain a more accurate estimation of the utility harmonic impedance. The results of the simulation and case study indicated that the traditional estimation methods have large errors when the background harmonic fluctuates significantly or the wind-farm-side harmonic impedance is smaller than the utility-side harmonic impedance. In contrast, the proposed method has a higher accuracy for the above scenarios.

INDEX TERMS D-PMSG wind farm, power quality, utility-side harmonic impedance wind-farm-side harmonic impedance.

I. INTRODUCTION

With the continuous development of power systems, nonlinear loads such as power electronic devices have gradually resulted in increasingly severe harmonic pollution problems [1]. Calculating the utility harmonic impedance at the point of common coupling (PCC) is a prerequisite for the division of harmonic responsibility [2]–[5]. The harmonics at the PCC of a wind farm are the result of the interaction of utility harmonic sources (background harmonics) in the internal and external systems of the wind farm. When background harmonics are too large to be ignored, the harmonic impedance on both sides at the PCC must be reasonably calculated and the level of harmonic emission evaluated [6], [7]. The wind-farm-side harmonic impedance is primarily determined using an inductance–capacitance–inductance (LCL) filter, reactive power compensation device, collector line, and transformer of the wind generator [8]. Because the amplitudes of the wind-farm-side and utility-side harmonic impedances are similar, the effects of harmonics on either side of the PCC must be considered simultaneously.

Existing methods for calculating utility-side harmonic impedance based on harmonic data at the PCC [9]–[23] primarily include the fluctuation method [9], linear regression method [10]–[12], independent random vector method [13], [14], independent component analysis [15]–[20], and modern class method [21]–[23].

The fluctuation method calculates the utility-side harmonic impedance based on the ratio of the harmonic voltage to the harmonic current at the PCC. Reference [9] proposed an improved fluctuation method based on the principle of phase angle correction. However, it requires that the harmonic source on the customer side has sufficient fluctuation and the system background harmonic is relatively stable, both of which are difficult to satisfy in an actual system.

The linear regression method calculates the utility-side harmonic impedance by solving the coefficient of the regression equation. Reference [11] proposed a method for

The associate editor coordinating the review of this manuscript and approving it for publication was Qiuye Sun.

measuring the utility harmonic impedance based on the complex data-oriented least-square regression. However, the method is invalid when the harmonic voltage and current at the PCC do not conform to a linear relationship. Additionally, the regression analysis becomes biased when the background harmonic is not normally distributed.

The independent random vector method evaluates the level of harmonic emission based on the near-independent covariance of the harmonic current at the PCC and the background harmonic voltage. Reference [13] estimated the utility harmonic impedance using this method. However, this method is valid on the premise that the harmonic impedance on the customer side is significantly greater than that on the utility side. Because the wind power generator filter has a low impedance at some harmonic frequencies, the correlation between the harmonic current and background harmonic is enhanced. Therefore, the independent analysis is biased.

The independent component analysis (ICA) method separates mixed signals based on independent or weak correlations of source signals and utilizes the similarity of historical data to create node matching [15]. Reference [16] proposed a practical harmonic impedance calculation method based on fast ICA, which reduced the disturbances of the utility harmonic to some extent. But this method also requires a high degree of independence between the harmonic voltage and current at the PCC. Data separation is difficult when background harmonics account for a large proportion of data. When the separated data are computed using the least-squares method, a large amount of data and various iterations are involved. If the initial values are set unreasonably, non-convergence may occur.

Modern class methods include the AR model and Burg algorithm [21], harmonic source fluctuation correlation [22], measured harmonic data correlations [23], etc. Reference [21] assumed that the voltage and current at the PCC satisfy the AR model and used the Burg algorithm to calculate the coefficients of the AR model. But the noise in the measured harmonics deteriorates the estimation results. Reference [22] used the correlation of fluctuations of the harmonic current on both sides of the PCC to calculate the utility harmonic impedance. However, the calculation results are influenced by the amplitude of the harmonic fluctuation energy. Reference [23] used the correlation of the harmonic data measured at the PCC to estimate the utility harmonic impedance, but the computational effort increased significantly when the correlation of harmonic data was enhanced.

To justify the novelty of the research work in this paper, Table 1 shows a comparison of the proposed method with four basic methods.

In summary, most of the existing methods require some mathematical assumptions, such as 1) the harmonic impedance on the customer side is significantly greater than that on the utility side [13], [14], 2) harmonic fluctuations on both sides of the PCC are independent [15], [16], and 3) harmonic data measured at PCC are correlated [22], [23].

TABLE 1. Method comparison.

Method and reference paper	Limitation	Novelty of the research work
Fluctuation [9]	This method requires sufficient fluctuation of harmonics on both sides of PCC	The proposed method is not affected by harmonic fluctuations on both sides of the PCC
Linear regression [11]	This method fails when the linear relationship between voltage and current no longer holds	The proposed method modifies the model with measured data, independent of the limitations of the system model. The harmonic currents and voltages at the PCC can conform to a nonlinear relationship
Independent random vector [13]	This method is based on the premise that the harmonic impedance on the customer side is much larger than that on the utility side	The proposed method has no requirement for the harmonic impedance on both sides of the PCC, and does not require the harmonic current to be approximately independent with the harmonic voltage
Independent component analysis [16]	When the difference between the harmonic impedances on the customer side and the utility side is very small, the calculation accuracy is reduced	The calculation results of the proposed method are not affected by the correlation of the amplitude of the harmonic impedance on both sides of the PCC

Because the installation of filters and reactive power compensators on the wind farm side decreases its harmonic impedance, the above assumptions do not hold true. Relatively few studies have been conducted on this subject. Existing methods are significantly limited by the accuracy of the system model in practical applications, and they lose validity when the preconditions are not satisfied. Based on the above background and requirements, this paper proposes a method based on a modified model with measured data to compensate for the limitations of the system model.

This paper proposes a utility impedance estimation method for a direct-drive permanent magnet synchronous generator (D-PMSG) wind farm based on a modified model with measured data. First, the component models of the wind farm were constructed, and the wind-farm-side harmonic impedance was calculated using the aggregation equivalent method. Subsequently, the Norton equivalent circuit is used to construct the estimation model for the utility harmonic impedance. The measured harmonic current and voltage at the PCC were processed using the random sample consensus (RANSAC) algorithm to correct the estimation model. Finally, a complex linear regression equation was

established, and the utility harmonic impedance was obtained using the complex least-squares method.

The innovation of this paper mainly lies in using the measured data to modify the model. The proposed method has no conditions for utility-side and wind-farm-side harmonic impedances. Simulation and field-testing results revealed that the proposed method can suppress the effect of background harmonics within a certain range, verifying its accuracy and feasibility.

II. PROBLEMS EXISTING IN TRADITIONAL MODELS TO ESTIMATE UTILITY HARMONIC IMPEDANCE

As shown in Fig. 1, the Norton equivalent circuit is utilized to calculate the utility-side harmonic impedance [20]–[23].

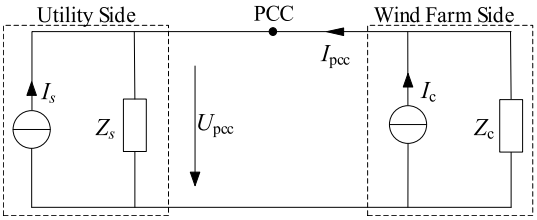

FIGURE 1. Equivalent circuit of the system and the wind farm.

In Fig. 1, I_s and I_c are the utility-side and wind-farm-side equivalent harmonic current sources, respectively. Z_s and Z_c are equivalent harmonic impedances. U_{pcc} and I_{pcc} are the harmonic voltage and harmonic current measured at the PCC, respectively.

The estimation accuracy of existing methods depends heavily on the mathematical assumptions of the models used. The fluctuation method requires sufficient fluctuation of the harmonics at the PCC; the linear regression method requires a linear relationship between the harmonic voltage and current at the PCC; the random independent vector method requires Z_c to be significantly larger than Z_s; the independent component method has deviations when the amplitude of Z_c is approximate to Z_s. In summary, the estimation accuracy of existing methods depends greatly on the limitations of its mathematical model. When the premises of the models cannot be satisfied, the estimation results have large errors. Z_c may be equal to or less than Z_s, based on the special characteristics of wind farm structures. Therefore, existing models for harmonic impedance estimation may lose their validity. Most of the above methods are based on models, whereas the accurate estimation of harmonic impedance requires a combination of correct mathematical models and measured data. According to the equivalent circuit, the following equations can be obtained:

$$U_{pcc} = \frac{Z_s Z_c}{Z_s + Z_c} I_c + \frac{Z_c Z_s}{Z_c + Z_s} I_s \tag{1}$$

$$I_{pcc} = \frac{Z_c}{Z_c + Z_s} I_c - \frac{Z_s}{Z_c + Z_s} I_s \tag{2}$$

Based on the equivalent circuit and (1) and (2), we can observe that the harmonic voltage and current at the PCC result from the interaction between the utility and the wind farm. The utility-side harmonic emission level (U_{pcc_s}) and wind-farm-side harmonic emission level (U_{pcc_c}) are defined as follows:

$$U_{pcc\_s} = \frac{Z_s Z_c}{Z_s + Z_c} I_s = \frac{U_s Z_c}{Z_s + Z_c} \tag{3}$$

$$U_{pcc\_c} = U_{pcc} - U_{pcc\_s} = \frac{Z_s Z_c}{Z_s + Z_c} I_c = \frac{Z_s U_c}{Z_s + Z_c} \tag{4}$$

where U_s and U_c are the utility-side and wind-farm-side harmonic voltages, respectively. Based on the principle of linear regression, there should be no correlation between the explanatory variables and regression coefficients. Therefore, in this study, we selected (2) to establish the regression equation. I_{pcc} was used as the dependent variable and I_c as the explanatory variable. The simulation results verified that there was a strong linear relationship between I_c and I_{pcc}.

To accurately estimate the utility-side harmonic impedance (Z_s) for a D-PMSG wind farm, we must calculate the wind-farm-side harmonic impedance (Z_c) in advance and measure the harmonic voltage and harmonic current at the PCC.

III. PROPOSED METHOD

A. HARMONIC IMPEDANCE MODEL OF THE WIND FARM

1) HARMONIC IMPEDANCE MODEL OF D-PMSG

The D-PMSG system consists of a rotor-side converter (RSC), grid-side converter (GSC), and a filter. The RSC and GSC of the D-PMSG are separated using direct current (DC) capacitors. Therefore, the harmonic impedance model of the D-PMSG is only determined using the harmonic characteristics of the GSC, control system, and filter. The D-PMSG harmonic impedance model is illustrated in Fig. 2.

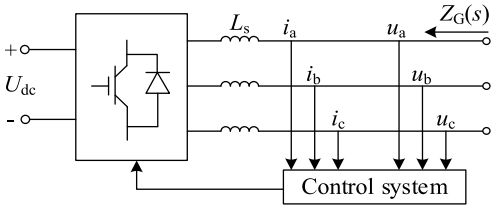

FIGURE 2. Harmonic impedance modal of D-PMSG.

where i_a, i_b, and i_c are the phase currents, u_a, u_b, and u_c are the phase voltages, U_{dc} is the DC side voltage, and L_s is the filter inductor. The inverter model from [24] was used with phase-domain current control, ignoring the phase-locked loop dynamics. The harmonic impedance of the D-PMSG can be calculated using

$$Z_G(s) = \frac{K_m U_{dc} H_i(s) G_i(s) + sL_s}{1 - K_m U_{dc} K_f(s) G_v(s)} \tag{5}$$

where K_m is the pulse width modulation modulator gain, $G_i(s)$ is the current sampling system delay, $G_v(s)$ is the voltage sampling system delay, $H_i(s)$ is the current control compensator and $K_f(s)$ is the feedforward gain.

2) HARMONIC IMPEDANCE MODEL OF REACTIVE POWER COMPENSATION EQUIPMENT

The static var generator (SVG) outputs the reactive current through the inverter. transformers are often connected after SVG as filter inductances to suppress the harmonics generated by the inverters of the SVG. Hence, the DC-side capacitor is connected to the external grid through the inverter, filter inductor, and three-phase transformer. The harmonic impedance of the SVG can be expressed as

$$Z_{\mathrm{SVG}}(s) = Z_{\mathrm{inv}}(s) + Z_{\mathrm{T}}(s) \tag{6}$$

where Z_{inv} and Z_{T} are the complex frequency-domain expressions for the harmonic impedance of the inverter and transformer, respectively. Z_{inv} can be calculated using (5). To calculate Z_{T}, it is necessary to determine the indefinite admittance matrix Y of the transformer in advance. Considering the frequency characteristics and the capacitive effect of the transformer, all the elements of the matrix were measured using the method in [25]. After obtaining the matrix Y, to solve Z_{T}, it is necessary to perform terminal elimination on Y, and maintain only the two terminals of the transformer connected to the external circuit. Here, Y is a 2×2 matrix, and Z_{T} is the negative reciprocal of the non-diagonal elements of Y.

$$Z_{\mathrm{T}} = -1/y_{12} = -1/y_{21} \tag{7}$$

3) EQUIVALENT HARMONIC IMPEDANCE MODEL OF A COLLECTOR LINE

We assume that the collector wires are connected in a hybrid manner. Cables are used between the generator and box transformer, and between the box transformer and the main transmission line. Overhead lines are used as the main transmission lines. Z_{f} is defined as the equivalent harmonic impedance of a single collector line, and can be expressed as follows:

$$Z_{\mathrm{f}} = \frac{Z_{\mathrm{G}} + Z_{\mathrm{N}}}{n} + Z_{\mathrm{M}} \tag{8}$$

where n is the total number of D-PMSGs on a single collector line, Z_{N} is the line connection impedance (cable impedance), and Z_{M} is the impedance of the main transmission line. Z_{N} can be calculated using

$$Z_{\mathrm{N}} \approx \sum_{i=1}^{n} iZ_i = nZ_{\mathrm{L}} - \sum_{i=1}^{n} (n-i)Z_i \tag{9}$$

where Z_i $(i = 1, 2, 3 \ldots n)$ is the cable impedance between adjacent generators, and its sum is the total cable impedance Z_{L}.

Using (9), the maximum and minimum values of Z_{N} can be obtained as

$$Z_{\mathrm{Nmax}} = nZ_L \ (Z_i = 0(i = 1, 2, \ldots, n-1), Z_n = Z_L) \tag{10}$$

$$Z_{\mathrm{Nmin}} = Z_{\mathrm{L}} \ (Z_i = 0(i = 2, 3, \ldots, n), Z_1 = Z_{\mathrm{L}}) \tag{11}$$

B. AGGREGATION EQUIVALENCE METHOD FOR WIND FARM

Accurately calculating the wind-farm-side harmonic impedance requires detailed modeling of all units, which requires a significant amount of computing resources. To simplify the calculation, the collector network of a wind farm is generally considered as a whole in practice, regardless of its internal details.

Therefore, this study utilized the aggregation equivalence method to simplify the wind farm network. The entire network is classified according to D-PMSG parameters, and the wind farm is considered as several generators with corresponding box transformers. The principles of equivalence are as follows: (1) The voltage, current, and power at the PCC of the wind field are constant before and after the aggregation, and (2) the unit capacity after aggregation should be equal to the detailed model.

This study classifies wind farms according to the type of generator used. We assume that there are p groups of different types of D-PMSGs in a wind farm. Subsequently, the entire collector network can be equivalent to a single collector line connecting the p groups of the generators with the corresponding box transformers. The aggregated harmonic impedance of the collector network Z_{feq} consists of p groups of wind power units and line-connection impedance.

$$Z_{\mathrm{feq}} = Z_{\mathrm{Geq}} + Z_{\mathrm{Neq}} \tag{12}$$

where Z_{Geq} is the total harmonic impedance of the aggregated wind power unit, and Z_{Neq} is the aggregated line-connection impedance. Z_{Geq} was obtained by paralleling the p groups of the different wind power units. To simplify the calculation process, we define Z_{Neq} as the mean of its maximum and minimum values, which are pZ_{Leqmax} and Z_{Leqmin}, respectively, from (10) and (11). Z_{Geq} and Z_{Neq} can be obtained using

$$Z_{\mathrm{Geq}} = 1/\sum_{i=1}^{p} \frac{1}{Z_{\mathrm{Geq}i} + Z_{\mathrm{BT}}} \tag{13}$$

$$Z_{\mathrm{Neq}} = \frac{pZ_{\mathrm{Leqmax}} + Z_{\mathrm{Leqmin}}}{2} = \frac{pZ_{\mathrm{L}} + Z_{\mathrm{L}}/p^2}{2} \tag{14}$$

where Z_{Geqi} is the total harmonic impedance of the aggregated wind power unit of group i, and Z_{BT} is the impedance of the corresponding box transformer.

When a D-PMSG ceases operation owing to faults or other reasons, if the same type of ceased D-PMSG exists in the wind farm, the number of equivalent wind power units p after aggregation remains unchanged. Only one aggregated equivalent wind power unit will be affected, and its corresponding Z_{Geqi} must be corrected. The topology of the equivalent network remains unchanged; thus, Z_{Neq} is consistent.

In summary, the wind-farm-side harmonic impedance can be expressed as

$$Z_{\mathrm{c}} = \frac{Z_{\mathrm{feq}} Z_{\mathrm{SVG}}}{Z_{\mathrm{feq}} + Z_{\mathrm{SVG}}} + Z_{\mathrm{ST}} \tag{15}$$

TABLE 2. All transformers used in the study.

Transformer types	Position	Purpose
SVG transformer	Connected to the DC capacitor in the SVG	Calculate the harmonic impedance of SVG
Step-up transformer	Connected between the wind-farm bus and the external grid	Calculate the wind-farm-side harmonic impedance
Box transformer	Connected after the D-PMSG turbine	Calculate the equivalent harmonic impedance of D-PMSG

where Z_{ST} is the short-circuit impedance of the step-up transformer. Note that the proposed aggregation equivalence method applies only to the D-PMSG wind farm. To enhance the readability of this article, all transformers used in this study are summarized in Table 2.

C. UTILITY HARMONIC IMPEDANCE ESTIMATION FOR A D-PMSG WIND FARM

Most existing methods are based on models, which can result in significant errors when the premises of the model cannot be satisfied. In this study, we utilized the measured harmonic data at the PCC to modify the traditional model. Therefore, the application of the utility harmonic impedance estimation was extended, and a more accurate estimation value was obtained. The following explains the specific correction steps.

Based on the fluctuation of data collected at the PCC, this study utilizes the RANSAC algorithm to process the measured U_{pcc} and I_{pcc} to reduce the error and obtain a value closer to the true value. In this study, the harmonic voltage and harmonic current are approximately linear. Therefore, the harmonic data were fitted as a straight line using the following equation: $Ax + By + C = 0$. The sample data (X) to be processed is presented as $X = \{(a_1 + jb_1, c_1 + jd_1) \ldots (a_n + jb_n, c_n + jd_n)\}$ and the distance (d_i) from other data points is calculated using the fitting model:

$$d_i = \frac{|A(a_i + jb_i) + B(c_i + jd_i) + C|}{\sqrt{A^2 + B^2}} (i = 1, 2, \ldots, n) \quad (16)$$

If $d_i \leq \delta$, then this point is considered as the 'inner point'. The threshold value (δ) is obtained as follows:

$$\delta = \frac{\sigma\sqrt{2\log(n)}}{\sqrt{n}} \quad (17)$$

where σ is the standard deviation of the measured data. After the algorithm ends, the new sample data are assumed to be N_{tol}. The signal selection criterion was constructed according to the RANSAC algorithm. A local search was performed on the fitted source signal, and the local signal with high coincidence to the source signal was selected, which created the data-filtering result closer to the true value. The algorithm steps are summarized as follows:

I. Assuming that a total of n data points are measured, the model to be fitted requires at least m points to decide ($m < n$) II. The iteration number is set to $k = 1$. III. Randomly select m points from n data points to fit the model. IV. Given a deviation δ, calculate the distance d_i from other points in the dataset to the fitted model. If $d_i < \delta$, then this data point is considered as the interior point; otherwise, it is considered as the exterior point. V. If the number of interior points exceeds the threshold, the algorithm ends. Otherwise, let $k = k+1$ and return to step III. If k exceeds a specified value, the algorithm ends, and the set of data points with the largest number of interior points is considered as the data filtering result.

The measured data in this study were the interacted harmonics for both the utility-side and wind-farm-side harmonics. The method for calculating the wind-farm-side harmonic impedance is described in section III. Subsequently, I_c can be obtained using

$$I_c = \frac{U_{pcc}}{Z_c} + I_{pcc} \quad (18)$$

A regression model is required to calculate the utility-side harmonic impedance. The slope of the fitted straight line was obtained using the complex least-squares method. Owing to errors in data collection and changes in the system state, the relationship between the I_{pcc} and I_c is expressed as follows:

$$I_{pcc} = \beta_1 I_c + \beta_0 + \varepsilon \quad (19)$$

where I_{pcc} is the dependent variable, I_c is the explanatory variable, β_1 and β_2 are the regression coefficients, and ε is the deviation between the predicted and true values. β_1 and β_2 can be obtained using

$$\beta_1 = \frac{Z_c}{Z_c + Z_s} \quad (20)$$

$$\beta_0 = -\frac{Z_s}{Z_c + Z_s} I_s \quad (21)$$

We assume that the original data of the I_{pcc} and U_{pcc} (n groups) are measured in a cycle. After processing using the RANSAC algorithm, the number of data groups was n_{tol}. The regression equation can be expressed as

$$\mathbf{y} = \mathbf{A}\mathbf{x} + \boldsymbol{\varepsilon} \quad (22)$$

$$\mathbf{y} = [I_{pcc}(1) I_{pcc}(2) \ldots I_{pcc}(n_{tol})]^T \quad (23)$$

$$\mathbf{A} = \begin{bmatrix} 1 & 1 & \ldots & 1 \\ I_c(1) & I_c(2) & \ldots & I_c(n_{tol}) \end{bmatrix}^T \quad (24)$$

$$\mathbf{x} = [\beta_0 \beta_1]^T \quad (25)$$

$$\boldsymbol{\varepsilon} = [\varepsilon(1) \varepsilon(2) \ldots \varepsilon(n_{tol})]^T \quad (26)$$

the sum of squares of deviation ε can be minimized as

$$\min \sum_{i=1}^{n_{tol}} \varepsilon_i^2$$

TABLE 3. Maximum harmonic distortion rate of utility grids.

Nominal voltage of power grid (kV)	Maximum harmonic distortion rate (%)
0.38	5.0
6	4.0
10	
35	3.0
66	
110	2.0

and $\mathbf{x}$ can be obtained using the complex least-squares method:

$$\mathbf{x} = (\overline{\mathbf{A}}^T \mathbf{A})^{-1} \overline{\mathbf{A}}^T \mathbf{y} \tag{27}$$

where $\overline{\mathbf{A}}$ is the conjugation of matrix $\mathbf{A}$. Subsequently, the utility-side harmonic impedance can be obtained using:

$$Z_s = \frac{Z_c(1-\beta_1)}{\beta_1} \tag{28}$$

Reference [26] demonstrated that harmonics gradually decrease during transmission from a low to a high voltage level. The regulation of the maximum harmonic distortion rate of the public power network in GBT14549-93 is presented in Table 3.

According to the law of decreasing harmonic transmission, the allowable values of harmonic distortion rate for voltage levels of 220 and 500 kV are set to 1.5% and 1.3%, respectively [27]. Therefore, this method is applicable to wind farms with a voltage level of 220 kV or below. When the voltage level is higher than 220 kV, the proposed method is no longer applicable because of the low harmonic distortion rate, which results in difficulty in obtaining harmonic data measurements. Additionally, the proportion of background harmonics increases in high-voltage networks.

Finally, a flow chart for estimating the utility harmonic impedance with a D-PMSG wind farm is presented in Fig. 3.

IV. ALGORITHM VALIDATION

A. ERRORS IN CALCULATING WIND-FARM-SIDE HARMONIC IMPEDANCE

A particular wind farm in China is considered as an example, and the parameters of the D-PMSG and LCL inverter are presented in Table 4. The generator and filter parameters were obtained from the corresponding nameplate, and the other parameters were obtained from actual measurements.

According to the parameters in Table 4 and the method proposed in reference [24], the parameters in (5) can be obtained, which further leads to $Z_G(s)$. The amplitude and phase of the harmonic impedance of each harmonic were estimated and compared with the actual values. In practical engineering, the inverter-side inductance (L_{inv}) and grid-side

TABLE 4. Parameters of PMSG generator and PMSG inverter.

Parameters	Value	Parameters	Value
Rated Power P (MW)	2.0	Filter Resistance R_h (Ω)	0.1
Rated Voltage U_g (kV)	0.69	Inverter Side Inductance L_{inv} (mH)	0.18
Filter Capacitor C_f (μF)	700	Grid Side Inductance L_g (mH)	0.04

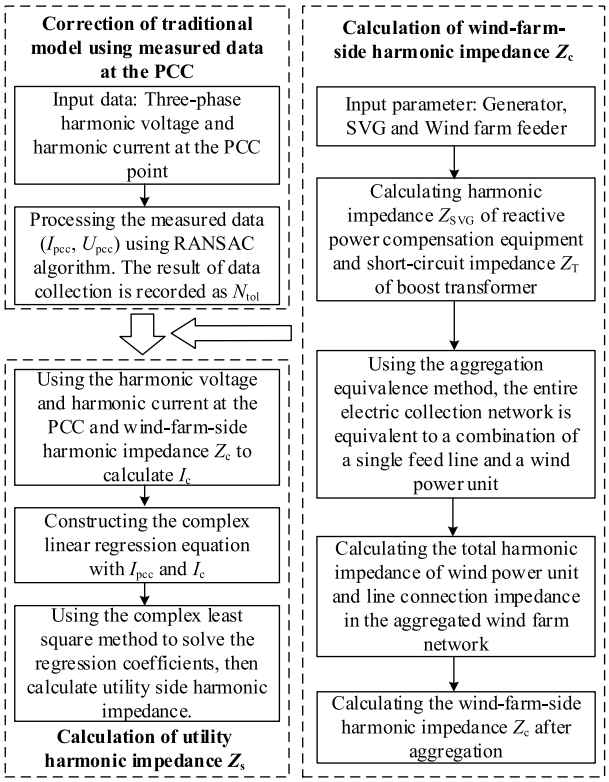

FIGURE 3. Flow-chart for estimating utility harmonic impedance for a D-PMSG wind farm.

inductance (L_g) of the LCL filter fluctuate. The inductance ratio (k) is defined as follows:

$$k = L_{inv}/L_g \tag{29}$$

Many measured parameters of the LCL filter have revealed that in actual wind farms, the range of k is frequently between 4 and 6. The impedance curves of the D-PMSG at different k values for each harmonic are shown in Fig. 4. For the 5th, 7th, 11th, and 13th harmonics, the actual harmonic impedance curve of the D-PMSG is within the upper and lower boundary curves.

The error of the line-connection impedance (Z_N) is analyzed as follows. The wind farm is assumed to consist of 25 generators and five collector wires that connect five generators. The length of the collector wire is 4.3, 9.1, 12.4, 14.5, and 16.2 km, respectively. The unit impedance of the collector line at a power frequency is 0.14+j0.33 Ω/km. The number, length, and unit impedance of the collector line

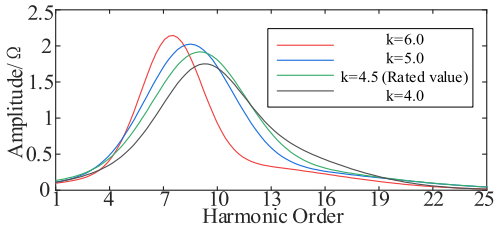

FIGURE 4. Amplitudes of the harmonic impedance of the D-PMSG at different inductance ratios.

TABLE 5. Accurate and equivalent values of the line-connection impedance.

The line-connection impedance Z_n in different harmonic orders (Ω)					
Harmonic order		5	7	11	13
Actual value	Scenario 1	1.5∠68°	7.3∠81°	4.6∠15°	1.6∠-31°
	Scenario 2	2.3∠68°	10∠81°	6.8∠15°	2.4∠-31°
	Scenario 3	0.3∠68°	1.5∠81°	0.9∠15°	0.3∠-31°
	Scenario 4	0.5∠68°	2.2∠81°	1.4∠15°	0.5∠-31°
Calculated value		1.3∠68°	6.2∠81°	3.9∠15°	1.4∠-31°

can be obtained by actual measurement. Z_L was assumed to contain ±20% fluctuations. The extreme conditions that may occur in the collector network were considered: Scenarios 1 and 2: the generators are all at the end of the collector line with the minimum or maximum Z_L; Scenarios 3 and 4: one generator is at the end, and the rest of the generators are at the top of the line with the minimum or maximum Z_L. The actual value of Z_N was calculated using (9). Z_{Neq} was calculated using the proposed aggregation-equivalent method. These two values are listed in Table 5.

As shown in Table 5, for the major harmonics, the calculated values of the connection impedance of the collector network lay between the boundaries of the actual values. Under normal operating conditions, the approximate calculation of the connection impedance of the collector network using the aggregation equivalent method has a certain accuracy. The error in the wind-farm-side harmonic impedance was then analyzed. Other wind farm parameters are listed in Table 6. The parameters of the step-up transformer, SVG, and SVG transformer were obtained from the corresponding nameplates. PCC parameters can be obtained by actual measurement.

The calculated and average values of the wind-farm-side harmonic impedance for a measured point located on the 35 kV bus are presented in Table 7. The calculated values were obtained using the proposed aggregation-equivalent method.

ε_c is the relative error of the amplitude of the wind-farm-side harmonic impedance. In an actual operation, Z_c is between the boundary values. A large amount of measured data revealed that Z_c is approximately normally distributed.

TABLE 6. Other parameters of the wind farm.

Parameters	Parameter Description
PCC	Rated voltage: 35 kV. Short-circuit capacity: 766 MVA
Step-up transformer	Rated voltage: 230/38.5 kV. Rated capacity: 100 MVA Short-circuit impedance of transformer: 6.6%. Short-circuit loss: 217 kW
SVG	Rated capacity: 9 MVA. Rated voltage: 10 kV
SVG transformer	Rated voltage: 38.5/10.5 kV. Rated capacity: 10 MVA Short-circuit impedance of transformer: 10%. Short-circuit loss: 60 kW

TABLE 7. Calculated and average values of the wind-farm-side harmonic impedance.

Harmonic order	Wind-farm-side harmonic impedance Z_c (Ω)			
	Maximum value	Minimum value	Average value	Calculated value
5	3.09∠86.5°	3.01∠87.9°	3.05∠87.2°	3.08∠87.2°
7	5.46∠85.8°	5.10∠87.3°	5.27∠86.4°	5.28∠86.2°
11	8.06∠71.8°	8.95∠83.6°	8.50∠77.4°	8.45∠77.2°
13	6.95∠81.5°	6.92∠86.2°	6.93∠83.9°	6.90∠83.8°

Hence, the probability of Z_c being near the mean value was the highest. Therefore, the true value is approximated using the average value. As Table 7 shows, the maximum values of ε_c for the 5th, 7th, 11th, and 13th harmonics were 4.0%, 16.3%, 6.3%, and 1.1%, respectively. The maximum amplitude error was 16.3%, which indicates that the proposed method for approximately calculating Z_c has some accuracy.

The various parameters of the components of a wind farm fluctuate. Therefore, the actual parameters deviate from the rated parameters, causing fluctuations in Z_c. Based on the actual operation of the wind farm, the parameters that fluctuate are assumed to be the D-PMSG inverter-side inductance (L_{inv}), D-PMSG inverter-side filter capacitance (C_f), and step-up transformer short-circuit impedance (Z_{ST}) [28].

L_{inv}, C_f, and Z_{ST} may simultaneously increase or decrease, respectively. The maximum fluctuations of L_{inv}, C_f, and Z_{ST} were assumed to be ±5%, ±5%, and ±10%, respectively [28]. Two extreme scenarios were considered: all three parameters were the maximum, or they were minimum. The boundary and estimated values of Z_c with the rated parameters are shown in Fig. 5. We observed that the estimated Z_c was within the upper and lower boundaries, which indicates that the proposed method has a certain accuracy under small parameter fluctuations. In addition, using the proposed method, Z_c can be calculated up to the 50th and even higher, but the harmonic impedance of the 2nd to the 25th can already reflect the accuracy of the proposed method.

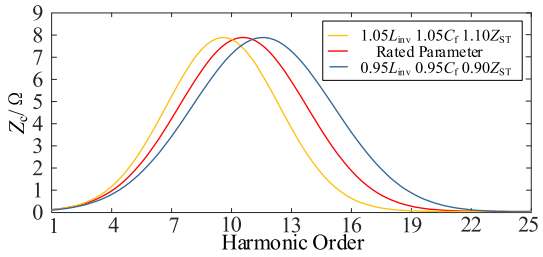

FIGURE 5. Amplitudes of Z_c when parameters fluctuate.

B. CALCULATION OF THE UTILITY-SIDE HARMONIC IMPEDANCE

In this section, Z_s is calculated using the simulation data. The error is solved by comparing it with the true value to verify the accuracy of the proposed method for calculating the utility-side harmonic impedance.

Simulations were performed using MATLAB R2019a. The simulation parameters were defined as follows:

1) Harmonic current: The amplitude of the wind-farm-side harmonic current (I_c) was 50 A with ±10% sinusoidal fluctuations and ±5% normal fluctuations. The phase angle was 30° with ±5% normal fluctuations. The amplitude of the utility-side harmonic current (I_s) was q times the I_c and the phase angle was set to 10°.
2) Harmonic impedance: The system-side harmonic impedance (Z_s) was 3+j4 Ω, and the wind-farm-side harmonic impedance (Z_c) was 2+j3 Ω.

A total of 1000 data points were simulated, and 100 points were considered as a group. The results of the proposed method were compared with four other methods (Methods 1 to 4 were the reference methods: the fluctuation, binary linear regression, independent random vector, and independent component methods. Method 5 is the proposed method). It is worth noting that no DC components are considered in the analysis of both simulation and field-testing data.

1) BACKGROUND HARMONICS ARE NORMALLY DISTRIBUTED

The amplitude and phase angle of I_s were assumed to contain ±5% normal random perturbations, and q increased gradually. As shown in Fig. 6, the error of Methods 1 to 3 increased significantly with the increase in background harmonics, whereas Method 5 was the least affected. This was because the linear relationship between I_{pcc} and U_{pcc} was weakened when the background harmonics increased, which resulted in higher errors in the fluctuation and binary linear regression methods. The independent random vector method approximated I_c with I_{pcc}, and the error increased with the fluctuation in I_{pcc}.

As q increases, the background harmonics increase, and the linear relationship between I_{pcc} and U_{pcc} is weakened. Scatter maps of the amplitudes of the I_{pcc} and U_{pcc} for different q values were plotted, and the correlation coefficients were calculated (Fig. 7).

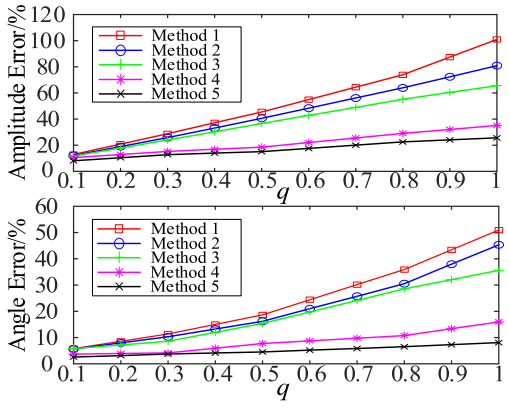

FIGURE 6. Errors of amplitude and angle of Z_s when background harmonics are normally distributed.

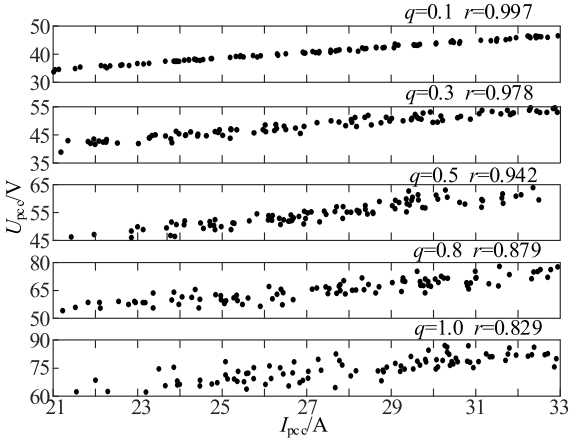

FIGURE 7. Amplitudes of I_{pcc} and U_{pcc} for different q values.

When $q = 0.1$–0.5, the correlation coefficient $r > 0.942$, the linear relationship between U_{pcc} and I_{pcc} was maintained, and Z_s was constant. When $q = 0.5$–1, r is between 0.942 and 0.829, the linear relationship gradually weakens, and the value of Z_s fluctuates slightly. When $q > 1$ and $r < 0.829$, the linear relationship disappears, and the value of Z_s is unstable. Because the RANSAC algorithm utilized in this study was a first-order fitting, the method failed when there was no linear relationship between U_{pcc} and I_{pcc}. Therefore, the proposed method is applicable only when $q < 1$.

In this study, the slope was calculated by constructing a first-order linear regression equation for I_c and I_{pcc} and further calculating Z_s. Therefore, it was necessary to verify the linear relationship between I_c and I_{pcc}. As q increases, the scatter plot between I_c and I_{pcc} is shown in Fig. 8, and the correlation coefficient (r) for different q values was calculated.

As shown in Fig. 8, the linear relationship between I_c and I_{pcc} decreases slightly as q increases, but generally maintains a good linear relationship. When q is less than 1, r is greater than 0.94. Therefore, when $q < 1$, the first-order linear regression equation for I_c and I_{pcc} is valid, and Z_s can be calculated by solving the regression coefficient β_1.

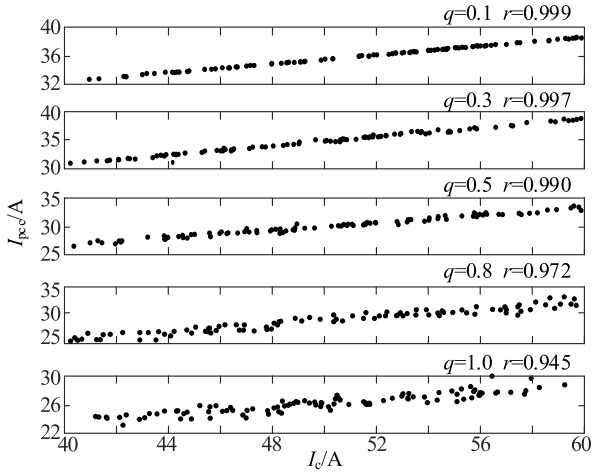

FIGURE 8. Amplitudes of I_c and I_{pcc} for different q values.

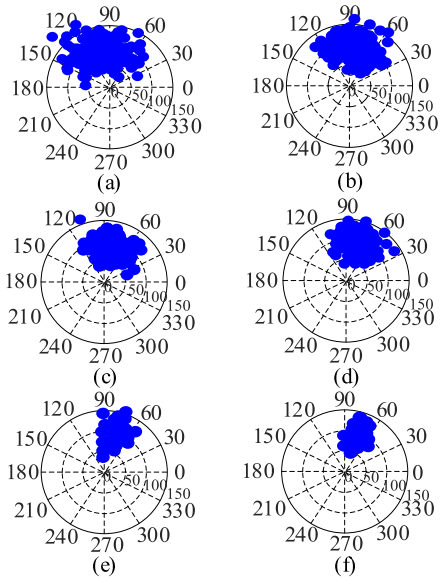

FIGURE 9. Polar coordinate diagrams of U_s when background harmonics are normally distributed. U_s calculated using (a) Method 1, (b) Method 2, (c) Method 3, (d) Method 4, and (e) Method 5. (f) Reference U_s.

Given that I_s is known, the value of U_s can reflect the accuracy of the Z_s calculation. The value of U_s can be calculated directly from the product of I_s and Z_s. To verify the validity and accuracy of the proposed method further, Fig. 9 shows the polar coordinate diagrams of U_s calculated using each method when $q = 0.5$, as well as the reference values of U_s (actual values).

As shown in Fig. 9, Method 5 exhibited the best consistency with the reference value. Method 1 required high accuracy for harmonic voltage and current. Therefore, the calculation results do not satisfy the requirements when the disturbance source fluctuates significantly at the PCC. Method 2 was also affected by inaccurate data, which resulted in a loss of robustness for the regression equation. Method 3 statistically suppressed the effects of the fluctuation of background harmonics on the estimation accuracy, but it required that the harmonic impedance on the wind farm side

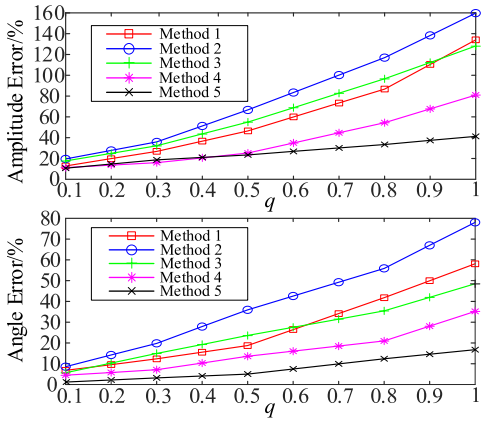

FIGURE 10. Errors of amplitude and angle of Z_s when background harmonics are non-normally distributed.

be significantly greater than that on the utility side. Based on the specific structure of the wind farm, the D-PMSG filter exhibited low impedance at some harmonic frequencies, which did not satisfy the precondition. Because Method 4 utilized the ICA algorithm, the result of data separation appeared as a singular solution in a few scenarios, which decreased the overall estimation accuracy. Method 5 uses the measured data to modify the model and is not affected by background harmonics. Therefore, the distributions of the amplitude and phase angle of the U_s obtained using Method 5 were closest to the true distributions, which verified the accuracy of the proposed method.

2) BACKGROUND HARMONICS ARE NON-NORMALLY DISTRIBUTED

The amplitude and phase angle of the I_s were assumed to contain ±5% sinusoidal fluctuations and ±5% normal random perturbations. The value of q gradually increased. As Fig. 10 shows, the errors of Methods 1 to 4 generally increased compared with the normally distributed background harmonic. That of Method 2 increased the most because the background harmonic impedance was not constant. Because the background harmonic could not be ignored here, the error of Method 1 increased significantly when q exceeded 0.5. Therefore, it is not advisable to consider only the wind-farm-side harmonics. As q increased gradually, the errors in Methods 1 to 4 increased significantly. The accuracy of Method 5 was higher than that of the other methods. Because the background harmonic was not normally distributed, the randomness and uncertainty of the harmonic emission increased, which increased the error of Method 4.

Similarly, Fig. 11 shows the polar coordinates of the values calculated using each method and the reference values (actual values) of the utility-side harmonic voltage when $q = 0.5$.

As shown in Fig. 11, for Methods 1 and 2, when the background harmonic was not normally distributed, the error in the calculation results of U_s increased significantly. This is because the fluctuation in the background harmonics increases further. Therefore, if the harmonic impedance is

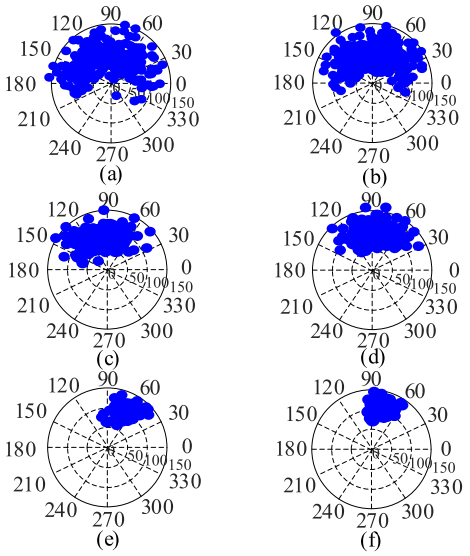

FIGURE 11. Polar coordinate diagrams of U_S when background harmonics are non-normally distributed. U_S calculated using (a) Method 1, (b) Method 2, (c) Method 3, (d) Method 4, and (e) Method 5. (f) Reference U_S.

solved using the ratio of the changing harmonic voltage to the harmonic current or by establishing a binary linear regression equation, the calculation results cannot satisfy the engineering requirements. The amplitude of Us calculated by Methods 3 and 4 was closer to the true value, but a phase error still occurred. In Method 3, the D-PMSG filter exhibited low impedance characteristics at certain harmonic frequencies. Additionally, the background harmonics were not normally distributed, and the wind-farm-side harmonic sources exhibited non-normal distributions at some harmonic frequencies. Thus, the approximate independency between the utility-side and wind-farm-side harmonic sources is weakened. Therefore, it is not feasible to eliminate the background harmonic correlation using covariance characteristics and then calculate the utility-side harmonic impedance. Method 4 also required that the harmonic sources on the utility side and wind-farm side change approximately independently. The ICA algorithm was required to decompose the fluctuating X–Y orthogonal component of the harmonic voltage and harmonic current at the PCC to obtain the independent component. The background harmonics which were non-normally distributed affected the separation of harmonic data at the PCC, which increased the calculation error. Method 5 is not disturbed by the background harmonics, so the non-normally distributed background harmonics do not affect the harmonic impedance estimates. Consequently, Method 5 exhibited the best consistency with the reference values.

C. ANALYSIS OF FIELD-TESTING DATA

The values of I_{pcc} and U_{pcc} were measured at a 150 kV bus outside a certain wind farm in China under the 11th harmonic. The sampling frequency was 5 kHz. The linear correlation coefficient between the I_{pcc} and U_{pcc} was calculated to be 0.9664. Therefore, there was a strong linear relationship

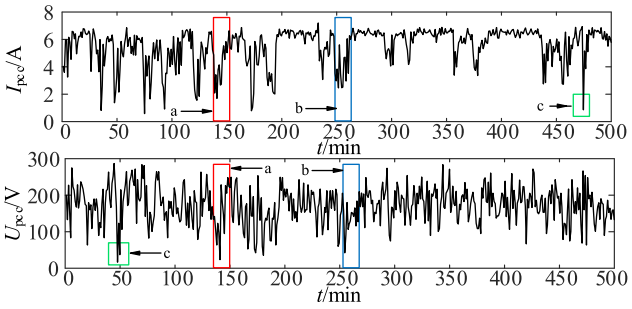

FIGURE 12. Measured values of 11th harmonic current and voltage.

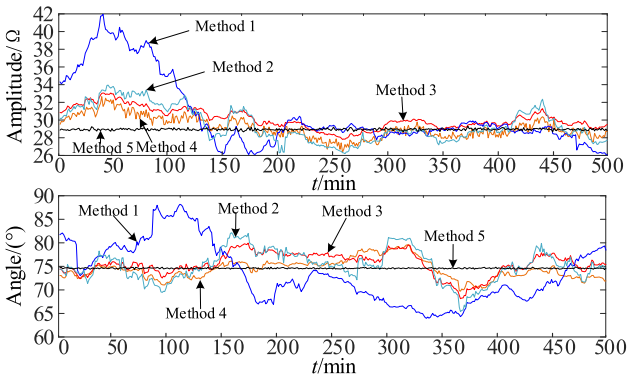

FIGURE 13. Estimated values of the 11th utility harmonic impedance.

between the I_{pcc} and U_{pcc}, and the proposed method was applicable. The value of Z_c was calculated to be 24.9∠18°Ω. The harmonic current and harmonic voltage were collected during the operating period of the wind farm (0–500 min). The collected data were processed using the RANSAC algorithm to obtain the utility-side harmonic impedance. Fig. 12 shows the measured 11th harmonic current and harmonic voltage at the PCC. Each point in the figure represents the average harmonic sampling data within 1 min.

For the collected harmonic data, the amplitude and phase angle of the utility-side harmonic impedance were calculated using Methods 1 to 5, respectively, to obtain the Z_s values within the measurement period, as shown in Fig. 13.

Owing to the stable operation of the entire system during data collection, U_{pcc} and I_{pcc} conform to a linear relationship. The change in Z_s is small; therefore, the accuracy of the proposed method can be guaranteed based on this feature. Because the ratio of U_{pcc} to I_{pcc} was relatively high in the first 100 data points, the amplitude and phase angle of Z_s calculated using Method 1 were significantly higher than those calculated using Methods 2 to 5. The amplitude and phase angle curves of Z_s obtained using Methods 2 to 4 were similar. As boxes a and b in Fig. 12 show, the values of U_{pcc} and I_{pcc} fluctuated significantly during this period, which resulted in a decrease in the linear relationship between the harmonic voltage and current. Therefore, the calculated values of the phase angle using Method 2 in these two periods were greater than those of the other methods.

As shown in Fig. 13, the amplitudes of the utility-side harmonic impedance fluctuated from 26 to 42 Ω, with an

average value of approximately 29 Ω. This does not satisfy the premise of Method 3; that is, the amplitude of Z_c should be significantly greater than Z_s. Therefore, the amplitude and phase angle of Z_s calculated using Method 3 fluctuated. Method 4 suppressed the fluctuations of the amplitude and phase angles of the harmonic sources to some extent and required no matching prior data. However, the accuracy for separating harmonic data measured from the PCC was easily affected, and the iteration speed for utilizing the data unmixing matrix was low, both of which increased the fluctuation of the calculated values. Additionally, for some abrupt harmonic signals with large variations (box c in Fig. 12, for example), it was difficult to determine the unmixed signal after inputting the observation signal. Therefore, the source signal could not be solved. These factors create difficulties for practical applications. The above evidence proves the accuracy and validity of the proposed method.

V. CONCLUSION

Most existing methods for estimating the utility harmonic impedance are based on models. When the premise of a model cannot be satisfied, the estimation results will have large errors. Owing to the installation of filters and reactive power compensation devices on the wind farm side, Z_c may be less than or equal to Z_s. This poses a challenge when estimating the utility harmonic impedance. In actual systems, the harmonic impedance cannot be solved based only on mathematical models. In this paper, a method of estimating the utility harmonic impedance for a D-PMSG wind farm based on a modified model with measured data is proposed, which overcomes the challenges of relying solely on models. The estimation results are not affected by the amplitudes of the harmonic impedances on both sides of the PCC. The effectiveness of the proposed method was confirmed using simulations and field-testing data. Back-to-back converters in wind farms may emit high-frequency harmonics during operation; thus, estimating the utility impedance in these high-frequency harmonics is a direction for further research.

REFERENCES

[1] A. Bozicek, J. Kilter, T. Sarnet, I. Papic, and B. Blazic, "Harmonic emissions of power electronic devices under different transmission network operating conditions," *IEEE Trans. Ind. Appl.*, vol. 54, no. 5, pp. 5216–5226, Sep. 2018.
[2] D. Saxena, S. Bhaumik, and S. N. Singh, "Identification of multiple harmonic sources in power system using optimally placed voltage measurement devices," *IEEE Trans. Ind. Electron.*, vol. 61, no. 5, pp. 2483–2492, May 2014.
[3] J. Meyer, A.-M. Blanco, M. Domagk, and P. Schegner, "Assessment of prevailing harmonic current emission in public low-voltage networks," *IEEE Trans. Power Del.*, vol. 32, no. 2, pp. 962–970, Apr. 2017.
[4] K. Tang and C. Shen, "Harmonic emission level assessment method based on parameter identification analysis," *IET Gener., Transmiss. Distribution*, vol. 13, no. 7, pp. 976–983, Apr. 2019.
[5] O. Unsar, O. Salor, I. Cadirci, and M. Ermis, "Identification of harmonic current contributions of iron and steel plants based on time-synchronized field measurements—Part I: At PCC," *IEEE Trans. Ind. Appl.*, vol. 50, no. 6, pp. 4336–4347, Dec. 2014.
[6] X. Zheng, X. Xiao, and Y. Wang, "An impedance matrix constrained-based method for harmonic emission level estimation," *Int. Trans. Electr. Energy Syst.*, vol. 30, no. 9, p. e12479, Sep. 2020.
[7] K. Zhu, Y. Wang, X. Lu, and J. C. M. Vieira, "A new DG anti-islanding protection technique based on harmonic impedance measurement," *Int. Trans. Electr. Energy Syst.*, vol. 27, no. 2, p. e2251, Feb. 2017.
[8] S. A. Papathanassiou and M. P. Papadopoulos, "Harmonic analysis in a power system with wind generation," *IEEE Trans. Power Del.*, vol. 21, no. 4, pp. 2006–2016, Oct. 2006.
[9] K.-L. Song, X.-D. Yuan, B. Chen, and S. Zhao, "A method for assessing customer harmonic emission level based on improved fluctuation method," in *Proc. China Int. Conf. Electr. Distrib.*, Sep. 2012, pp. 1–5.
[10] T. Zang, Z. He, L. Fu, Y. Wang, and Q. Qian, "Adaptive method for harmonic contribution assessment based on hierarchical *K*-means clustering and Bayesian partial least squares regression," *IET Gener., Transmiss. Distrib.*, vol. 10, no. 13, pp. 3220–3227, Oct. 2016.
[11] J. Hui, W. Freitas, J. C. M. Vieira, H. Yang, and Y. Liu, "Utility harmonic impedance measurement based on data selection," *IEEE Trans. Power Del.*, vol. 27, no. 4, pp. 2193–2202, Oct. 2012.
[12] X. Zheng, X. Xiao, and Y. Wang, "Harmonic impedance measurement based on an improved binary regression algorithm and dynamic time warping distance," *Int. J. Electr. Power Energy Syst.*, vol. 130, Sep. 2021, Art. no. 106907.
[13] J. Hui, H. Yang, S. Lin, and M. Ye, "Assessing utility harmonic impedance based on the covariance characteristic of random vectors," *IEEE Trans. Power Del.*, vol. 25, no. 3, pp. 1778–1786, Jul. 2010.
[14] Z. Zhong, Y. Zheng, and M. Xiong, "Assessment method of wind farm harmonic emission level based on improved covariance characteristic of random vectors," in *Proc. China Int. Conf. Electr. Distrib. (CICED)*, Sep. 2018, pp. 448–452.
[15] E. Gursoy and D. Niebur, "Harmonic load identification using complex independent component analysis," *IEEE Trans. Power Del.*, vol. 24, no. 1, pp. 285–292, Jan. 2009.
[16] X. Zhao and H. G. Yang, "A new method to calculate the utility harmonic impedance based on FastICA," *IEEE Trans. Power Del.*, vol. 31, no. 1, pp. 381–388, Feb. 2016.
[17] F. Karimzadeh, S. Esmaeili, and S. H. Hosseinian, "A novel method for noninvasive estimation of utility harmonic impedance based on complex independent component analysis," *IEEE Trans. Power Del.*, vol. 30, no. 4, pp. 1843–1852, Aug. 2015.
[18] F. Chen, N. Mao, Y. Wang, Y. Wang, and X. Xiao, "Improved utility harmonic impedance measurement based on robust independent component analysis and bootstrap check," *IET Gener., Transmiss. Distrib.*, vol. 14, no. 5, pp. 910–919, Mar. 2020.
[19] F. Karimzadeh, S. Esmaeili, and S. H. Hosseinian, "Method for determining utility and consumer harmonic contributions based on complex independent component analysis," *IET Gener., Transmiss. Distrib.*, vol. 10, no. 2, pp. 526–534, 2016.
[20] J. Zhao, H. Yang, A. Pan, and F. Xu, "An improved complex ICA based method for wind farm harmonic emission levels evaluation," *Electr. Power Syst. Res.*, vol. 179, Feb. 2020, Art. no. 106105.
[21] Q. Shu, Y. Fan, F. Xu, C. Wang, and J. He, "A harmonic impedance estimation method based on AR model and Burg algorithm," *Electr. Power Syst. Res.*, vol. 202, Jan. 2022, Art. no. 107568.
[22] Q. Shu, T. Liu, and F. Xu, "A new algorithm for calculating utility harmonic impedance," *Electr. Power Syst. Res.*, vol. 191, Feb. 2021, Art. no. 106893.
[23] Q. Shu, Y. Wu, F. Xu, and H. Zheng, "Estimate utility harmonic impedance via the correlation of harmonic measurements in different time intervals," *IEEE Trans. Power Del.*, vol. 35, no. 4, pp. 2060–2067, Aug. 2020.
[24] M. Cespedes and J. Sun, "Impedance modeling and analysis of grid-connected voltage-source converters," *IEEE Trans. Power Electron.*, vol. 29, no. 3, pp. 1254–1261, Mar. 2014.
[25] B. Gustavsen, "Wide band modeling of power transformers," *IEEE Trans. Power Del.*, vol. 19, no. 1, pp. 414–422, Jan. 2004.
[26] E. E. Ahmed, W. Xu, and G. Zhang, "Analyzing systems with distributed harmonic sources including the attenuation and diversity effects," *IEEE Trans. Power Del.*, vol. 20, no. 4, pp. 2602–2612, Oct. 2005.
[27] G. Mazzanti, "Reliability evaluation of insulation subjected to harmonic voltages within the limits set by international standards," *IEEE Trans. Dielectr. Elect. Insul.*, vol. 21, no. 5, pp. 2037–2046, Oct. 2014.
[28] H. García, J. Segundo, O. Rodríguez-Hernández, R. Campos-Amezcua, and O. Jaramillo, "Harmonic modelling of the wind turbine induction generator for dynamic analysis of power quality," *Energies*, vol. 11, no. 1, p. 104, Jan. 2018.